

Tumor Targeting by an Aptamer

Brian J. Hicke¹; Andrew W. Stephens¹; Ty Gould¹; Ying-Fon Chang¹; Cynthia K. Lynott¹; James Heil¹; Sandra Borkowski²; Christoph-Stephan Hilger²; Gary Cook¹; Stephen Warren¹; and Paul G. Schmidt¹

¹NeXstar Pharmaceuticals, Boulder, Colorado; and ²Schering AG, Berlin, Germany

Aptamers are small oligonucleotides that are selected to bind tightly and specifically to a target molecule. We sought to determine whether aptamers have potential for in vivo delivery of radioisotopes or cytotoxic agents. **Methods:** TTA1, an aptamer to the extracellular matrix protein tenascin-C, was prepared in fluorescent and radiolabeled forms. After in vivo administration, uptake and tumor distribution of Rhodamine Red-X-labeled aptamer was studied by fluorescence microscopy. In glioblastoma (U251) and breast cancer (MDA-MB-435) tumor xenografts, biodistribution and imaging studies were performed using TTA1 radiolabeled with ^{99m}Tc. Tenascin-C levels and tumor uptake were studied in a variety of additional human tumor xenografts. To assess the effect of radiometal chelate on biodistribution, mercapto-acetyl diglycine (MAG₂) was compared with diethylenetriaminepentaacetic acid and with MAG₂-3,400-molecular-weight PEG (PEG_{3,400}). **Results:** Intravenous injection of fluorescent aptamer TTA1 produced bright perivascular fluorescence in a xenografted human tumor within 10 min. In the ensuing 3 h, fluorescence diffused throughout the tumor. Labeled with ^{99m}Tc, TTA1 displayed rapid blood clearance, a half-life of less than 2 min, and rapid tumor penetration: 6% injected dose (%ID)/g at 10 min. Tumor retention was durable, with 2.7 %ID/g at 60 min and a long-lived phase that stabilized at 1 %ID/g. Rapid tumor uptake and blood clearance yielded a tumor-to-blood ratio of 50 within 3 h. Both renal and hepatic clearance pathways were observed. Using the ^{99m}Tc-labeled aptamer, images of glioblastoma and breast tumors were obtained by planar scintigraphy. Aptamer uptake, seen in several different human tumors, required the presence of the target protein, human tenascin-C. Modification of the MAG₂ radiometal chelator dramatically altered the uptake and clearance patterns. **Conclusion:** TTA1 is taken up by a variety of solid tumors including breast, glioblastoma, lung, and colon. Rapid uptake by tumors and rapid clearance from the blood and other nontarget tissues enables clear tumor imaging. As synthetic molecules, aptamers are readily modified in a site-specific manner. A variety of aptamer conjugates accumulate in tumors, suggesting imaging and potentially therapeutic applications.

Key Words: SELEX; imaging; extracellular matrix; tenascin-C; oligonucleotide

J Nucl Med 2006; 47:668–678

Molecular targeting is of great interest for diagnosis and therapy, particularly in oncology. In contrast to perfusion-based imaging, molecular targeting is founded on the principle of high-affinity ligand binding to a macromolecule within a tissue of interest. Monoclonal antibodies (mAbs), because of their high affinity, specificity, and wide range of available targets, have been the workhorse of molecular targeting. Although successes have been documented, mAbs have a long blood residence, which decreases in vivo image quality. As a result, intact mAbs are becoming obsolete for in vivo imaging. In therapy, mAbs have the advantage of a higher uptake in target tissue, but long blood residence often causes dose-limiting hematologic toxicities. In addition, antibodies show incomplete penetration into target tissues. Therefore, new targeting agents and clinical protocols are needed. Examples include the use of smaller antibody fragments (1,2) and peptides (3), as well as antibody pretargeting strategies (4,5). Here, we describe the use of an aptamer now in clinical trials for specific targeting to tumor stromal elements.

As oligonucleotide ligands, aptamers are comparable to antibodies in specificity and affinity for their target molecule, typically a protein (6,7). At 8–15 kDa, aptamers are intermediate in size between antibodies (150 kDa) and small peptides (1–5 kDa) and are slightly smaller than single-chain variable-fragment antibodies (scFvs, 25 kDa). As polyanions, aptamers are quite different in composition from scFvs. As synthetic molecules, aptamers readily support site-specific modifications that maintain structure and activity. Aptamers can be coupled to diagnostic or therapeutic agents and to bioconjugates, such as polyethylene glycol (PEG) polymers, that can alter aptamer pharmacokinetics (8). Previous therapeutic work with aptamers has focused on blocking protein function; by far the most advanced work is represented by the use of a vascular endothelial growth factor aptamer, pegaptanib sodium (Macugen; Pfizer and Eyetech) (9), now approved for treatment of macular degeneration (10). In contrast to aptamers that block protein function, an aptamer that delivers radionuclides and chemotherapeutics was investigated in the experiments described here.

To effectively deliver a compound, a molecular targeting agent must accumulate to a significant degree in the pathologic tissue. In addition, the ratio between pathologic and normal tissues must be high. For successful in vivo imaging, the targeting agent should not reside long in the blood or in

Received Aug. 4, 2005; revision accepted Sep. 15, 2005.

For correspondence or reprints contact: Brian J. Hicke, Global Technologies (NZ) Ltd., 218 George St., P.O. Box 941, Dunedin 9001, New Zealand.

E-mail: bhicke@gmail.com

the organs of metabolism. The small size and polyanionic nature of aptamers may lead to rapid blood clearance and tissue uptake and may minimize the residence in liver and kidney, providing some potentially useful features for imaging and radiotherapy (11–13). Initial experiments to address aptamer suitability for in vivo imaging have been reported (14), as have studies designed to elucidate oligonucleotide biodistribution properties (15,16). To describe the molecular targeting properties of an aptamer in a human tumor xenograft model, we chose a previously selected aptamer with high affinity for a protein, tenascin-C, that is overexpressed in tumor tissues (17).

As a target protein, tenascin-C is distinguished by 2 features: abundance and accessibility to circulating ligands. Tenascin-C is a large ($>10^6$ Da) hexameric extracellular matrix protein that is newly expressed during tissue remodeling processes including angiogenesis, embryonic development, wound healing, and tumor growth (18–21). Tenascin-C is also overexpressed in the inflammatory foci of atherosclerosis (22). In contrast to restricted expression in normal tissues, inflammatory conditions, and wound healing, tenascin-C is abundantly and continuously expressed in neovasculature and tumor stroma. For example, tenascin-C was measured at approximately 1 $\mu\text{mol/L}$ within a human osteosarcoma (23); there are 6 aptamer binding sites per tenascin-C molecule (17). Tumors known to overexpress tenascin-C include carcinomas of the lung, breast, prostate, and colon, as well as lymphomas, sarcomas, glioblastomas, and melanomas. Antibodies against tenascin-C are capable of imaging human brain tumors (24,25). Because of its overexpression in many tumor types, its abundance, and its accessibility to circulating ligands, we chose tenascin-C for evaluation of aptamer-based tumor targeting.

The modified RNA aptamer, TTA1, was previously isolated using systematic evolution of ligands by exponential enrichment (SELEX) against tumor cells and purified tenascin-C (17). This aptamer has improved characteristics relative to an initial tenascin-C aptamer, discovered in a SELEX experiment targeting U251 glioblastoma cells (26). TTA1 binds with a dissociation constant of 5 nmol/L to the fibrinogen-like domain of tenascin-C. For protection against nucleases, the aptamer contains maximal 2'-OMe purine substitutions, 2'-F pyrimidines, and a 3'-3' inverted phosphodiester linkage. Finally, the synthetic aptamer was produced with a 5' amine to serve as a conjugation site. Unlike most protein constructs, the aptamer has a unique conjugation site. No bioconjugate we have tested has altered aptamer affinity for tenascin-C. The aptamer is therefore adaptable to different labeling strategies, described here, to determine its tumor-targeting characteristics.

MATERIALS AND METHODS

Oligonucleotide Synthesis

2'-Fluoropyrimidine phosphoramidite monomers were obtained from JBL Scientific; 2'-OMe purine, 2'-OH purine, hexyl amine, and $(\text{CH}_2\text{CH}_2\text{O})_6$ monomers, along with the polystyrene solid sup-

port that initiates the synthesis with a 3'-3' linkage, were obtained from Glen Research. Procedures were performed as previously described (27).

Oligonucleotide Conjugations

TTA1 and TTA1.NB were conjugated to the technetium chelator MAG_2 (28), through the 5' amine, at a 50 mg/mL aptamer in 30% dimethylformamide with 5 molar equivalents of MAG_2 succinimidyl ester buffered in sodium borate (100 mmol/L, pH 9.3), for 30 min at room temperature. Reversed-phase high-performance liquid chromatography purification (29) yielded MAG_2 -TTA1 and MAG_2 -TTA1.NB. For fluorescence studies, oligonucleotides were conjugated to Rhodamine Red-X succinimidyl ester (Molecular Probes, Inc.) using the above conditions for conjugation and high-performance liquid chromatography purification, to produce TTA1-Red or TTA1.NB-Red. Unlike fluorescein, the conjugated Rhodamine Red-X greatly increased retention time during reversed-phase high-performance liquid chromatography, enabling efficient separation of conjugated and unconjugated aptamer. Diethylenetriaminepentaacetic acid (DTPA) was coupled to the oligonucleotide 5' amine as previously described (30). The succinimidyl ester of MAG_2 -3,400-molecular-weight PEG ($\text{PEG}_{3,400}$) was prepared as follows: $\text{PEG}_{3,400}$ -N-hydroxysuccinimide (NHS) was reacted with an excess of Fmoc-Lys(NH_2)-COOH in acetonitrile with 10 molar equivalents of triethylamine. After extraction to remove free Fmoc-Lys(NH_2)-COOH, Fmoc was removed with 20% piperidine in acetonitrile and the product was precipitated in ether, dried under a vacuum, and then reacted with an excess of NHS- MAG_2 in acetonitrile with 10 molar equivalents of triethylamine. After a second extraction, the MAG_2 - $\text{PEG}_{3,400}$ was activated with DCC and NHS-OH, and the product was purified by filtration and extraction. The resulting NHS-activated MAG_2 - $\text{PEG}_{3,400}$ was precipitated in ether and dried under a vacuum. Conjugation to oligonucleotides was performed as described for MAG_2 .

Radiolabeling

Oligonucleotides were labeled with $^{99\text{m}}\text{Tc}$ in the following manner: to 1 nmol MAG_2 aptamer (or MAG_2 - $\text{PEG}_{3,400}$ aptamer) were added 200 μL of NaPO_4 buffer (100 mmol/L, pH 8.5), sodium tartrate (23 mg/mL), and 50 μL of pertechnetate in saline ($^{99\text{m}}\text{Tc}$, 185 MBq) eluted from a ^{99}Mo column (Syncor) within 12 h of use. The labeling reaction was initiated by the addition of 10 μL of SnCl_2 (5 mg/mL). The reaction mixture was incubated for 15 min at 90°C, cooled to 25°C, and spin filtered (0.1- μm Ultrafree [Millipore], 5 min at 4,000 rpm) to remove any particulates or precipitated material. Oligonucleotide was separated from unreacted $^{99\text{m}}\text{Tc}$ by spin dialysis through a 30,000-molecular-weight cutoff membrane (Centrex; Schleicher and Schuell) followed by three 300- μL washes and resuspension of the oligonucleotide in 100 μL of H_2O . This labeling protocol results in incorporation of 30%–50% of the added $^{99\text{m}}\text{Tc}$, with a specific activity of 74–111 MBq/nmol of DNA. ^{111}In labeling was performed as previously described (30). For ^{32}P labeling, the oligonucleotides were phosphorylated with polynucleotide kinase (New England Biolabs) using manufacturer-recommended conditions. The oligonucleotides, having a 5' amine, could be kinased (inefficiently) at the available hydroxyl group of the 3'-3' linkage. Aptamer affinities were determined by nitrocellulose filter partitioning using either ^{32}P -labeled or $^{99\text{m}}\text{Tc}$ -labeled aptamer and purified human tenascin-C (Chemicon). The antibodies BC-8 (kindly provided by Luciano Zardi, Laboratory of Cell Biology, Istituto Nazionale per la Ricerca

sul Cancro, Genoa, Italy), mTN12 (Sigma-Aldrich), and IgG (Sigma-Aldrich) were labeled with ^{125}I -*N*-succinimidyl-3-(4-hydroxyphenyl)propionate (Bolton-Hunter reagent; Amersham Pharmacia) according to manufacturer instructions.

Aptamer Biodistribution

Six- to 10-wk-old female nude mice (*nu/nu*; Taconic) received a subcutaneous injection of 10^6 human tumor cells into the flank. Tumors were allowed to grow to 200–350 mg—typically, for 10–30 d. Each mouse was briefly placed under a heat lamp to dilate the tail vein. A 200- μL volume of Dulbecco's phosphate-buffered saline (Gibco BRL) containing 0.5 nmol of $^{99\text{m}}\text{Tc}$ -labeled oligonucleotide (37–55.5 MBq) was mixed with 4.5 nmol of unlabeled oligonucleotide and injected into the tail vein using a 0.5-mL insulin syringe, to produce a 5-nmol (3.25 mg/kg) dose of the 13-kDa aptamer. At specified times, 3 mice were anesthetized with vaporized isoflurane (Aerrane; Baxter), and 200 μL of blood were collected by cardiac puncture. After cervical dislocation, tissues were collected and weighed, and γ -radioactivity was determined using a scintillation counter. All procedures on animals were performed according to the standards of the institutional animal care and utilization committee.

Tumor Imaging

Tumor-bearing mice received an injection of $^{99\text{m}}\text{Tc}$ -labeled aptamer or control aptamer as just described. At specified times, the mice were continuously anesthetized with vaporized isoflurane and imaged on a LEM+ γ -camera (Siemens) for 20 min. Images were presented using Nuclear MAC software (version 2.9; Scientific Imaging, Inc.) and Photoshop (version 5.5; Adobe Systems Inc.). Because aptamer clearance or metabolism was altered in animals that recovered from continuous anesthesia, the animals used for imaging were different from those used for biodistribution experiments.

Fluorescence Microscopy and Immunostaining

Nu/nu mice bearing U251 human glioblastoma tumors weighing 200–350 mg received a 5-nmol (3.25 mg/kg) injection of TTA1-Red or TTA1.NB-Red in 200 μL of Dulbecco's phosphate-buffered saline, along with 50 nmol of nonbinding carrier oligonucleotide (unlabeled TTA1.NB) that was included to slow aptamer clearance mechanisms. At specified times, the animals were anesthetized, perfused with saline, and killed. Tumors were harvested, placed in liquid optimal-cutting-temperature medium (Ted Pella Inc.), and frozen for storage at -80°C . Frozen sections 10 μm thick were then cut and surveyed by fluorescence microscopy. Immunostaining of human tenascin-C was performed according to manufacturer instructions (M.O.L. Staining Procedure, PK-2200; Vector Laboratories). Briefly, slides with mounted frozen sections were warmed to 25°C , incubated for 5 min in cold acetone, rinsed 2 times for 2 min each in H_2O , incubated with 0.1% hydrogen peroxide in 0.3% normal horse serum for 20 min, rinsed in phosphate-buffered saline, blocked for 60 min with mouse IgG blocking reagent, and washed. Antibody specific for human tenascin-C (BC-24, T-2551; Sigma-Aldrich) was diluted 1:1,600 in antibody diluent and incubated with the slide for 30 min. The slides were washed, incubated with biotinylated antimouse IgG, and washed and stained first with Vectastain ABC and then with peroxidase substrate 3',3'-diaminobenzidine (DAB substrate kit, SK-4100; Vector Laboratories). Finally, the slides were counterstained with hematoxylin, dehydrated, and mounted for microscopy. Immunostaining of mouse tenascin-C was identical except that before incubation with rat antimouse tenascin antibody (MTn-12,

T-3413; Sigma-Aldrich), the slides were blocked with Super Block (Pierce Biotechnology). The primary antibody was diluted 1:200 in antibody diluent, and the biotinylated antirat antibody (E0468; Dako) was diluted 1:400 before washing and staining.

Antibody Blotting

Total tumor protein was extracted from tumor xenografts with a sodium dodecylsulfate-containing protein sample buffer using a dounce homogenizer and centrifuged to remove insoluble material. Purified human tenascin-C was obtained from Chemicon. Cell culture supernatant from mouse 3T12 fibroblast cells (American Type Culture Collection) was obtained and stored frozen. Then, 10 μg of tumor protein extract, 10 μg of 3T12 cell supernatant protein, and 1 μg of purified human tenascin-C were separated on a 10% polyacrylamide sodium dodecylsulfate precast gel (Novex; Invitrogen) and electrophoretically transferred to nitrocellulose (Novex). The membrane was blocked overnight at 4°C in Tris-buffered saline (20 mM Tris, 150 mmol/L NaCl, pH 8.3) with 0.05% polysorbate-20 (Pierce) and 0.05% casein (w/v, I-block; Tropix). Blocking solution was replaced with a 1:2,000 dilution of antibody (mTN12 rat ascites fluid; Sigma), or mouse mAb BC-8 (Prof. Luciano Zardi, Laboratory of Cell Biology, Istituto Nazionale per la Ricerca sul Cancro, Genoa, Italy) for 3 h at room temperature followed by three 20-min washes with Tris-buffered saline–polysorbate. To detect bound antibody, blots were incubated for 90 min with a 1:25,000 dilution of goat antirabbit IgG (Sigma) or goat antimouse IgG, each conjugated to horseradish peroxidase, and washed 5 times for 5 min in Tris-buffered saline–polysorbate. Color was developed using chemiluminescence according to manufacturer instructions (Amersham Pharmacia).

RESULTS

Aptamer Tumor Uptake and Localization: Fluorescence Staining

Aptamer TTA1 is a 13-kDa oligonucleotide that binds tightly to tenascin-C (dissociation constant, 5×10^{-9} mol/L) (17). A nonbinding control aptamer, TTA1.NB, lacks 5 critical nucleotides (Fig. 1). A 5' amine, introduced synthetically, provides a conjugation site for the amine-reactive fluorophore and radiometal chelators indicated in Figure 1. The tumor model chosen for these studies, U251, is a human glioblastoma cell line xenografted to the flank of nude mice. Tumor uptake and localization were initially determined by injecting a fluorescent aptamer, TTA1-Red (Fig. 1), into tumor-bearing mice. After sacrifice of the animals, tumors were excised, frozen, and sectioned for fluorescence microscopy and immunohistochemical analysis (Fig. 2). Figure 2A shows microscopic tumor sections stained with hematoxylin and eosin. Ex vivo antibody staining, Figures 2B and 2C, revealed abundant tenascin-C (both species' isoforms) in the tumor stroma, including perivascular distribution. Ten minutes after injection of aptamer, there was intense tumor staining consistent with accumulation in the perivascular space (Fig. 2D). The control aptamer showed no staining (Fig. 2E). Within 3 h, aptamer was no longer confined to the site of its initial binding but instead diffused throughout the tumor stroma (Fig. 2F). The resulting staining pattern was consistent with that of tenascin-C in the extracellular matrix.

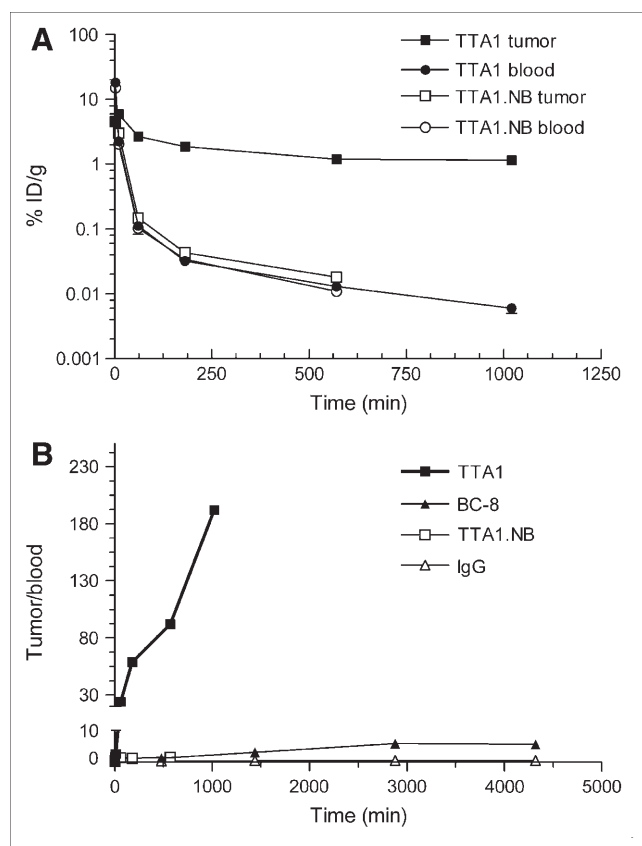


FIGURE 3. Plots of tumor and blood levels of aptamer (A) and tumor-to-blood ratio for aptamer and antibody (B) vs. time. Aptamers (TTA1 and control aptamer TTA1.NB) and antibody (BC-8 and control IgG) were radiolabeled with ^{99m}Tc and ^{125}I , respectively. Rapid ^{99m}Tc radioactive decay combined with extensive clearance of aptamer-associated ^{99m}Tc from blood prevented measurement of aptamer-associated ^{99m}Tc beyond 1,200 min.

liver at 10 min. After 3 h, radioactivity moved from the small intestine (dropping to 1–1.5 %ID/g) into the large intestine to a level of 35–40 %ID/g. In comparing the 2 clearance pathways, we found that approximately 50% of the injected ^{99m}Tc was cleared renally and that most of the remainder was cleared through the hepatobiliary system. Radioactivity was almost undetectable in blood, lung, and muscle after 3 h. Greater than 95% of the ^{99m}Tc had cleared from the body by 24 h. The biodistributions of binding and nonbinding aptamers were similar in nontumor tissues.

At 3 h after injection, radioactivity that remained in the plasma could not be precipitated with ethanol (data not shown). Therefore, this remaining radioactivity represented aptamer that was degraded into low-molecular-weight metabolites. In contrast, aptamer that extravasated into the tumor remained 60% intact at 3 h as judged by the ethanol precipitation assay (data not shown).

Aptamer Dose Response

To test aptamer biodistribution in response to dose level, we injected ^{99m}Tc -labeled TTA1 or TTA1.NB at 0.0325, 0.325, and 3.25 mg/kg. The dose was increased by the

addition of nonradiolabeled aptamer to a 0.0325 mg/kg dose of the radiolabeled aptamer. In this experiment, tumor uptake levels were similar to the initial biodistribution; however, clearance was not as rapid. The dose response (Table 2) indicated a striking effect: At 3 h, the 100-fold higher dose produced an approximately 3-fold increase in %ID/g. Blood levels increased slightly at 2 min and 10 min but were equivalent at later times. Taken together, increased tumor uptake and equivalent 3-h blood levels produced an increase in tumor-to-blood ratio from 14 to 38.

Aptamer Uptake into a Variety of Tumor Types

We found that the aptamer effectively targeted a variety of tumors. Human tumor xenografts including colon (SW620), breast (MDA-MB-468, MDA-MB-435), glioblastoma (U251), rhabdomyosarcoma (A673), and squamous cell carcinoma of the head and neck (KB) were tested. TTA1 accumulation at 3 h varied from 0.1 to 1.9 %ID/g depending on the tumor (Fig. 5A). In these tumor xenografts, both human (Fig. 5B) and mouse (Fig. 5C) tenascin-C were expressed. An exception was KB. This tumor did not express human tenascin-C and, uniquely, did not display aptamer uptake. TTA1 displayed 20-fold reduced binding to murine versus human tenascin-C (17). Because the KB tumor did not express human tenascin-C and did not show aptamer uptake, the data indicate that aptamer tumor targeting required binding of the target protein.

In Vivo Tumor Imaging

As the high tumor-to-blood ratios of TTA1 suggested, tumor images could be generated using aptamer TTA1. Using a γ -camera, scintigraphic images of U251 tumor-bearing mice were collected at time points identical to those for the biodistribution data (Fig. 6A). The images reflected what was observed by harvesting the tissues: At 10 min, the bladder and liver were predominant, reflecting the 2 major clearance pathways. Images of binding and nonbinding aptamer were similar, and the tumor just became visible on the animal's flank. At 3 h, the intestines were prominent, with bladder still evident for both binding and control aptamers. The tumor was clearly revealed by TTA1. In images taken at 18 h (Fig. 6A), radioactivity had almost entirely cleared the body, and the tumor was the brightest structure visualized. Finally, a breast tumor generated using the cell line MDA-MB-435 was imaged at 18 h (Fig. 6B), again demonstrating the ability of the aptamer to recognize multiple tumor types.

Altering Biodistribution: Radiometal Chelator Modification

We investigated the effects of radiometal chelator alterations on aptamer biodistribution. The first modification switched the TTA1 chelator to DTPA (Fig. 1), a highly anionic moiety. The second modification altered the previous MAG_2 chelator by insertion of a $\text{PEG}_{3,400}$ spacer between chelator and aptamer (Fig. 1). Figure 7 compares the biodistribution of $\text{MAG}_2(^{99m}\text{Tc})$ -TTA1, $\text{DTPA}(^{111}\text{In})$ -TTA1, and $\text{MAG}_2(^{99m}\text{Tc})$ - $\text{PEG}_{3,400}$ -TTA1 at 3 h. MAG_2 -TTA1

TABLE 1
Biodistribution of TTA1 and Control (TTA1.NB) Aptamers

Tissue	Time* (min)	TTA1		TTA1.NB	
		Mean (\pm SE) %ID/g	Tumor-to-tissue ratio	Mean (\pm SE) %ID/g	Tumor-to-tissue ratio
Tumor	2	4.47 \pm 0.41	1.0	4.51 \pm 0.30	1.0
	10	5.94 \pm 0.59	1.0	3.02 \pm 0.21	1.0
	60	2.69 \pm 0.31	1.0	0.15 \pm 0.02	1.0
	180	1.88 \pm 0.10	1.0	0.04 \pm 0.00	1.0
	570	1.20 \pm 0.07	1.0	0.02 \pm 0.00	1.0
	1,020	1.15 \pm 0.06	1.0	NA	
Blood	2	18.25 \pm 1.14	0.2	15.01 \pm 0.51	0.3
	10	2.27 \pm 0.25	2.6	2.05 \pm 0.20	1.5
	60	0.11 \pm 0.00	24.0	0.10 \pm 0.02	1.4
	180	0.03 \pm 0.00	58.8	0.03 \pm 0.00	1.3
	570	0.01 \pm 0.00	92.2	0.01 \pm 0.00	1.6
	1,020	0.01 \pm 0.00	202.5	NA	
Lung	2	8.97 \pm 1.21	0.5	8.13 \pm 0.96	0.6
	10	2.13 \pm 0.08	2.8	1.94 \pm 0.23	1.6
	60	0.16 \pm 0.01	17.1	0.12 \pm 0.01	1.2
	180	0.05 \pm 0.01	39.2	0.04 \pm 0.00	1.0
	570	0.03 \pm 0.01	42.8	0.02 \pm 0.00	1.1
	1,020	0.01 \pm 0.00	173.9	NA	
Liver	2	9.12 \pm 0.53	0.5	7.90 \pm 0.35	0.6
	10	12.46 \pm 1.25	0.5	9.10 \pm 0.83	0.3
	60	1.23 \pm 0.09	2.2	0.42 \pm 0.10	0.3
	180	0.40 \pm 0.08	4.7	0.21 \pm 0.06	0.2
	570	0.10 \pm 0.02	11.5	0.06 \pm 0.00	0.3
	1,020	0.07 \pm 0.00	15.4	NA	
Spleen	2	5.10 \pm 0.41	0.9	4.86 \pm 0.13	0.9
	10	2.46 \pm 0.21	2.4	1.22 \pm 0.12	2.5
	60	0.64 \pm 0.08	4.2	0.11 \pm 0.02	1.3
	180	0.20 \pm 0.03	9.5	0.04 \pm 0.01	1.1
	570	0.06 \pm 0.00	19.3	0.02 \pm 0.00	0.9
	1,020	0.03 \pm 0.00	38.7	NA	
Kidney	2	44.43 \pm 4.28	0.1	54.47 \pm 1.21	0.1
	10	18.81 \pm 0.94	0.3	14.32 \pm 2.08	0.2
	60	1.51 \pm 0.04	1.8	0.64 \pm 0.11	0.2
	180	0.29 \pm 0.03	6.6	0.22 \pm 0.02	0.2
	570	0.14 \pm 0.01	8.6	0.10 \pm 0.01	0.2
	1,020	0.08 \pm 0.01	14.1	NA	
Sm. int.	2	3.69 \pm 0.25	1.2	3.12 \pm 0.10	1.4
	10	7.01 \pm 0.07	0.8	6.44 \pm 0.25	0.5
	60	15.72 \pm 2.04	0.2	14.65 \pm 0.53	0.0
	180	1.48 \pm 0.71	1.3	1.24 \pm 0.41	0.0
	570	0.22 \pm 0.15	5.5	0.16 \pm 0.07	0.1
	1,020	0.28 \pm 0.24	4.1	NA	
Lg. int.	2	2.34 \pm 0.24	1.9	2.28 \pm 0.18	2.0
	10	0.89 \pm 0.04	6.7	0.77 \pm 0.07	3.9
	60	10.80 \pm 5.38	0.2	21.66 \pm 11.68	0.0
	180	26.18 \pm 7.84	0.1	18.02 \pm 3.49	0.0
	570	1.26 \pm 0.71	0.9	0.72 \pm 0.18	0.0
	1,020	0.30 \pm 0.17	3.9	NA	
Muscle	2	1.27 \pm 0.13	3.5	1.49 \pm 0.05	3.0
	10	0.87 \pm 0.09	6.8	1.84 \pm 1.00	1.6
	60	0.06 \pm 0.00	42.0	0.05 \pm 0.00	2.9
	180	0.02 \pm 0.00	117.7	0.01 \pm 0.00	3.9
	570	0.01 \pm 0.00	109.0	0.01 \pm 0.00	2.6
	1,020	0.00 \pm 0.00	420.3	NA	

*Time at which animals were anesthetized, blood was collected, animals were killed, tissues were weighed, and radioactivity was quantified in γ -counter. $n = 3$ mice per interval.

Sm. int. = small intestine; Lg. int. = large intestine.

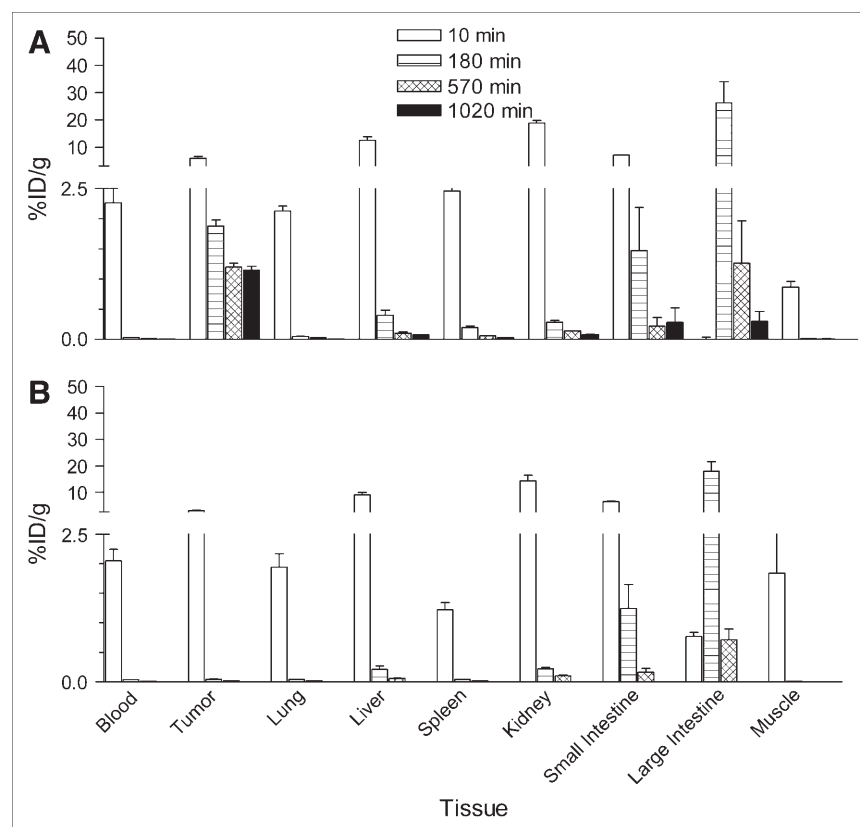


FIGURE 4. Bar graphs of aptamer bio-distribution in U251 tumor-bearing nude mice after a 3.25 mg/kg (5 nmol) intravenous injection of ^{99m}Tc -labeled TTA1 (A) and control nonbinding aptamer, TTA1.NB (B). Data are mean \pm SE. SE data are in Table 1.

showed its characteristically high intestinal accumulation. Conjugated to the aptamer, $\text{DTPA-}^{111}\text{In}$ abolished hepatobiliary clearance; instead, we observed increased and persistent accumulation in the liver and kidney. The radiolabel accumulated rapidly in the kidney to about 15 %ID/g (Fig. 7). This level was maintained for at least 24 h.

We hypothesized that inserting PEG between the chelate and the aptamer (Fig. 1) might increase the hydrophilicity of the metabolic product and thereby alter the biodistribution. Indeed, with insertion of a $\text{PEG}_{3,400}$ linker, hepatobiliary clearance was no longer observed (Fig. 7). ^{99m}Tc accumulated to a high degree in the kidney (21 %ID/g). However, in contrast to $\text{DTPA-}^{111}\text{In}$, this level represented transient passage through the kidney into the urine: By 17 h, no residual radioactivity remained in the kidney (data not shown). The conclusions for both chelators were supported by animal images obtained at 10 min, 1 h, and 3 h (data not shown). Taken together, the data indicate that simple and accessible changes to the radiometal chelator can have significant effects on tissue uptake and clearance patterns.

DISCUSSION

When fluorescently labeled and injected intravenously into tumor-bearing mice, aptamer TTA1 escapes the vasculature within 10 min, binding to tenascin-C-rich extracellular matrix immediately adjacent to the vessels. The aptamer has a dissociation constant of 5 nmol/L and the target is dense (1–10 $\mu\text{mol/L}$), suggesting the possibility of slow interstitial

diffusion (32), a so-called binding site barrier. Instead, between 10 min and 3 h, the aptamer diffuses significantly as judged by the fluorescent images. The affinity, target density, and size of the targeting molecule can separately affect uptake and diffusion rate within a tumor (32,33). The relatively rapid k_{on} and k_{off} ($2 \times 10^5 \text{ M}^{-1} \text{ s}^{-1}$ and $1 \times 10^{-3} \text{ s}^{-1}$, respectively) (17) and small size (13 kDa) of the aptamer may individually contribute to the observed rapid diffusion. Because the target protein is hexameric, conversion to a bivalent aptamer (similar to a bivalent antibody) may affect uptake levels and the intratumoral diffusion rate. Regardless of mechanism, this relatively small (13 kDa) and polyanionic targeting agent displays an interesting property: The circulating species, and associated bioconjugate, diffuses into the tumor from the initial extravasation site within 3 h. This feature may be of interest for therapeutic applications, such as for coupling to cytolytic compounds or to α -emitting radioisotopes with short half-lives, short pathlengths within tissues ($<100 \mu\text{m}$), and high energy emission (34).

Aptamer uptake by tumors was also studied using a ^{99m}Tc -radiolabeled form. A maximal tumor uptake of 6 %ID/g was observed rapidly, within 10 min, and was then found to be 1.9 %ID/g at 3 h. The control aptamer also showed high initial uptake (3 %ID/g at 10 min), but in contrast to TTA1, it washed out of the tumor rapidly (0.04 %ID/g at 3 h). Blood clearance was extremely rapid, leading to tumor-to-blood ratios of 50 within 3 h and 180 at 16 h. Together with the

TABLE 2
Biodistribution of ^{99m}Tc -Labeled Aptamer TTA1 in Response to Increasing Dose

Tissue	Time* (min)	0.0325 mg/kg		0.325 mg/kg		3.25 mg/kg	
		Mean (\pm SE) %ID/g	Tumor-to- blood ratio	Mean (\pm SE) %ID/g	Tumor-to- blood ratio	Mean (\pm SE) %ID/g	Tumor-to- blood ratio
Tumor	2	2.45 \pm 0.186	0.1	2.41 \pm 0.209	0.1	3.10 \pm 0.304	0.1
	10	2.12 \pm 0.653	1.6	4.08 \pm 0.269	2.9	4.40 \pm 0.212	2.7
	60	0.90 \pm 0.215	4.6	1.63 \pm 0.117	8.0	2.50 \pm 0.262	15.4
	180	0.68 \pm 0.046	14.3	1.45 \pm 0.296	27.9	1.96 \pm 0.068	38.4
Blood	2	16.95 \pm 2.900		19.70 \pm 3.520		23.70 \pm 2.020	
	10	1.35 \pm 0.233		1.41 \pm 0.076		1.64 \pm 0.123	
	60	0.20 \pm 0.048		0.20 \pm 0.025		0.16 \pm 0.008	
	180	0.05 \pm 0.005		0.05 \pm 0.003		0.05 \pm 0.003	
Lung	2	7.91 \pm 1.170		9.91 \pm 1.520		10.10 \pm 1.130	
	10	1.38 \pm 0.138		1.80 \pm 0.197		1.47 \pm 0.091	
	60	0.41 \pm 0.040		0.40 \pm 0.025		0.50 \pm 0.080	
	180	0.16 \pm 0.004		0.13 \pm 0.019		0.16 \pm 0.037	
Liver	2	36.38 \pm 2.630		22.60 \pm 1.580		10.50 \pm 1.270	
	10	46.60 \pm 11.000		32.10 \pm 1.210		10.80 \pm 1.030	
	60	12.30 \pm 2.010		12.20 \pm 1.500		5.44 \pm 0.197	
	180	3.22 \pm 0.162		2.27 \pm 0.261		1.45 \pm 0.152	
Spleen	2	14.88 \pm 0.92		11.20 \pm 1.25		6.28 \pm 0.88	
	10	17.40 \pm 3.04		12.00 \pm 1.57		3.45 \pm 0.15	
	60	5.57 \pm 1.45		4.62 \pm 0.55		1.73 \pm 0.10	
	180	1.09 \pm 0.14		1.21 \pm 0.16		0.545 \pm 0.02	
Kidney	2	52.72 \pm 5.93		51.10 \pm 4.30		45.7 \pm 3.65	
	10	31.50 \pm 8.91		68.60 \pm 3.40		39.8 \pm 1.23	
	60	5.47 \pm 1.66		15.40 \pm 1.13		13.8 \pm 3.37	
	180	1.05 \pm 0.08		4.60 \pm 0.08		4.63 \pm 0.62	
Sm. int.	2	4.49 \pm 0.35		3.91 \pm 0.40		3.74 \pm 0.43	
	10	3.06 \pm 0.73		3.73 \pm 0.45		4.29 \pm 0.65	
	60	27.10 \pm 3.96		22.70 \pm 1.17		15.6 \pm 2.24	
	180	5.33 \pm 1.04		6.08 \pm 2.04		2.23 \pm 0.40	

*Time at which animals were anesthetized, blood was collected, animals were killed, tissues were weighed, and radioactivity was quantified in γ -counter. $n = 3$ mice per interval.

Sm. int. = small intestine.

fluorescent staining patterns, these data demonstrate rapid extravasation, rapid blood clearance, and durable tumor retention, suggesting a potential match with short-lived radio-labeled species such as common isotopes used in PET.

As judged by an ethanol precipitation assay, the aptamer is rapidly degraded in blood. In contrast, aptamer that has entered the tumor remains largely intact, indicating that on extravasation the aptamer has reached a privileged site for protection from nuclease activity. This is consistent with data indicating that the majority of blood-borne oligonucleotide is degraded on passage through the liver (Andrew Stephens, unpublished data, June 1996). Two primary mechanisms operate simultaneously to remove TTA1-associated ^{99m}Tc from blood: renal filtration of intact aptamer and metabolites, and biliary excretion of the remaining metabolites.

We found an effect of aptamer dose on tumor uptake and tumor-to-tissue ratios. Slight increases of ^{99m}Tc in blood at 2 and 10 min suggested that intact aptamer levels might be

higher at increased doses and, thus, that there exists a saturable clearance mechanism or nuclease activity (14) operating in the first minutes after aptamer injection. Notably, the effect of increased dose is mimicked by the addition of a nonbinding carrier oligonucleotide (unlabeled TTA1.NB; data not shown). This increased accumulation with the addition of unlabeled aptamer appears counterintuitive. However, it can be understood in the context of a rapid and saturable clearance mechanism and high concentration of target protein in the tumor. Increasing the dose results in a greater circulating blood level; with a large excess of target protein in the tumor, increased blood levels result in increased tumor accumulation. Regardless of mechanism, the ability of a nonbinding oligonucleotide to boost early blood levels and tumor uptake may be useful clinically: Aptamer uptake into the target tissue could be increased by coadministration of a readily available, cost-effective generic-sequence oligonucleotide.

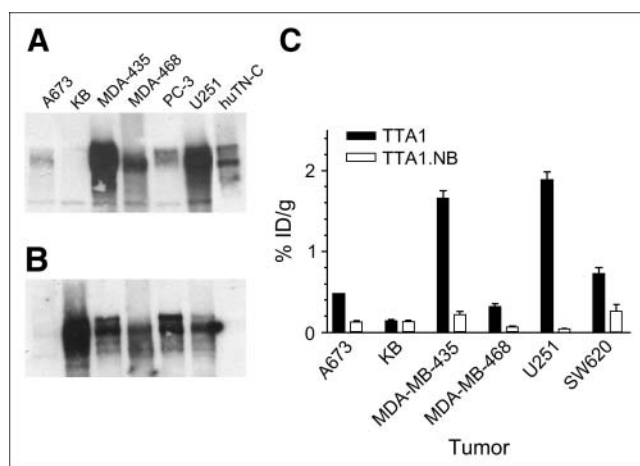


FIGURE 5. Tenascin-C expression and aptamer uptake into a variety of solid tumors. (A and B) Blots probed with antibody BC-8, specific for human tenascin (A), or antibody mTN12, specific for mouse tenascin (B). Purified human tenascin-C was present as control, for which large and small splice isoforms are evident. (C) Bar graph showing %ID/g in the various tumors. Data are mean \pm SE ($n = 3$). A673 = rhabdomyosarcoma; KB = squamous cell carcinoma of head and neck; MDA-MB-435 = breast tumor; MDA-MB-468 = breast tumor; PC-3 = prostate tumor; SW620 = colon tumor; U251 = glioblastoma.

In evaluating aptamers as tissue-targeting agents, we would have found scFv (25 kDa) or small peptide ligands (~ 1 kDa) to the same target protein to be useful, but they were not available. For comparison, however, a high-affinity scFv to an oncofetal fibronectin reached a maximum of 8 %ID/g at 3 h with a tumor-to-blood ratio of 1.9 at 3 h (35). Both scFv and aptamer develop high tumor-to-blood ratios over time, with the scFv reaching 12 at 24 h and the aptamer reaching 50 within 3 h and 180 at 16 h. Therefore, scFv uptake and clearance kinetics are intermediate between antibody and aptamer. In summary, aptamer TTA1 reaches high tumor-to-blood ratios relative to the antibody and scFv, and the kinetics are rapid, being comparable instead to small peptides (3).

Tenascin-C is overexpressed in many solid tumors, and the aptamer effectively targets a variety of tumor types. A correlation exists between levels of human tenascin-C expression and uptake of aptamer. The KB tumor, uniquely, does not express human tenascin-C and consequently displays no aptamer uptake. Thus, these data demonstrate 3 salient features of TTA1-based tumor targeting: Uptake is strictly dependent on the presence of the target protein, a wide variety of tumors are clinical candidates for in vivo imaging with TTA1, and high-affinity binding is necessary to achieve accumulation at the target site.

As a target protein, the abundant and hexameric extracellular matrix protein tenascin-C can be contrasted to sparsely expressed proteins, such as growth factors. Specificity of expression makes some growth factors, such as vascular endothelial growth factor, attractive targets. It will be of interest to compare imaging agents that are targeted to

abundant versus rare target proteins. Low levels of tenascin-C expression occur in some normal tissues such as skin, kidney, and liver, leading one to question—in considering tenascin-C as a target protein—whether the aptamer might target normal tissues in humans. However, tenascin-C levels in normal tissues are far below those seen in pathologic tissues, as has been demonstrated in histochemical staining experiments (36) and in our Western blotting experiments (data not shown). Further, target accessibility to circulating ligands is of paramount importance: The aptamer may be cleared before it reaches sites that are less well perfused (37). A combination of tissue accessibility and target abundance, absent in most normal tissues, may be critical for developing high target-to-blood ratios.

When radiolabeled with ^{99m}Tc , aptamer TTA1 displays both renal and hepatobiliary clearance. Because of nucleolytic degradation in blood, clearance patterns may be dominated by aptamer metabolites. If so, insertion of a hydrophilic linker between aptamer and radiometal chelator might alter the biodistribution pattern. Indeed, substitution of DTPA- ^{111}In or insertion of a PEG_{3,400} linker dramatically reduced hepatobiliary clearance. The DTPA- ^{111}In aptamer displayed persistent kidney uptake: Similar behavior is seen with DTPA- ^{111}In -labeled peptides and antibody fragments, which are filtered by the glomerulus and reabsorbed in the proximal tubule. There, the molecules are metabolized. The chelate ^{111}In - ϵ -lysine appears to be the dominant retained metabolite (38–40). A similar process may be occurring with DTPA-conjugated aptamers, where the most likely breakdown products include the chelated radiometal, linkage, and perhaps 5'-terminal nucleotides. With the PEG linker, renal clearance predominated and was transient, representing passage into urine rather than uptake by the kidneys. These experiments support previous observations that oligonucleotides conjugated with MAG3 versus hydrazinonicotinamide (15) display different biodistributions. Because of DNA oligonucleotide degradation, the observed clearance patterns are dominated by the chelator. Taken together, the data indicate that simple and accessible changes to the radiometal chelator can have significant effects on tissue uptake and clearance patterns.

CONCLUSION

As a target, tenascin-C is expressed abundantly in many tumors at sites that are directly accessible to circulating aptamer, enabling TTA1 uptake into a variety of tumor types including glioblastoma, breast, and colon. Aptamer-based tumor targeting has 2 distinct phases: rapid access (shared by binding and nonbinding species) followed by durable retention within the tumor (binding aptamer only). Rapid uptake, rapid blood clearance, and high tumor-to-blood ratios enable scintigraphic imaging within 60 min of injection. Instead of remaining at the site of entry, the aptamer diffuses throughout the tumor stroma. Modifying the radiometal chelator dramatically alters tissue uptake and

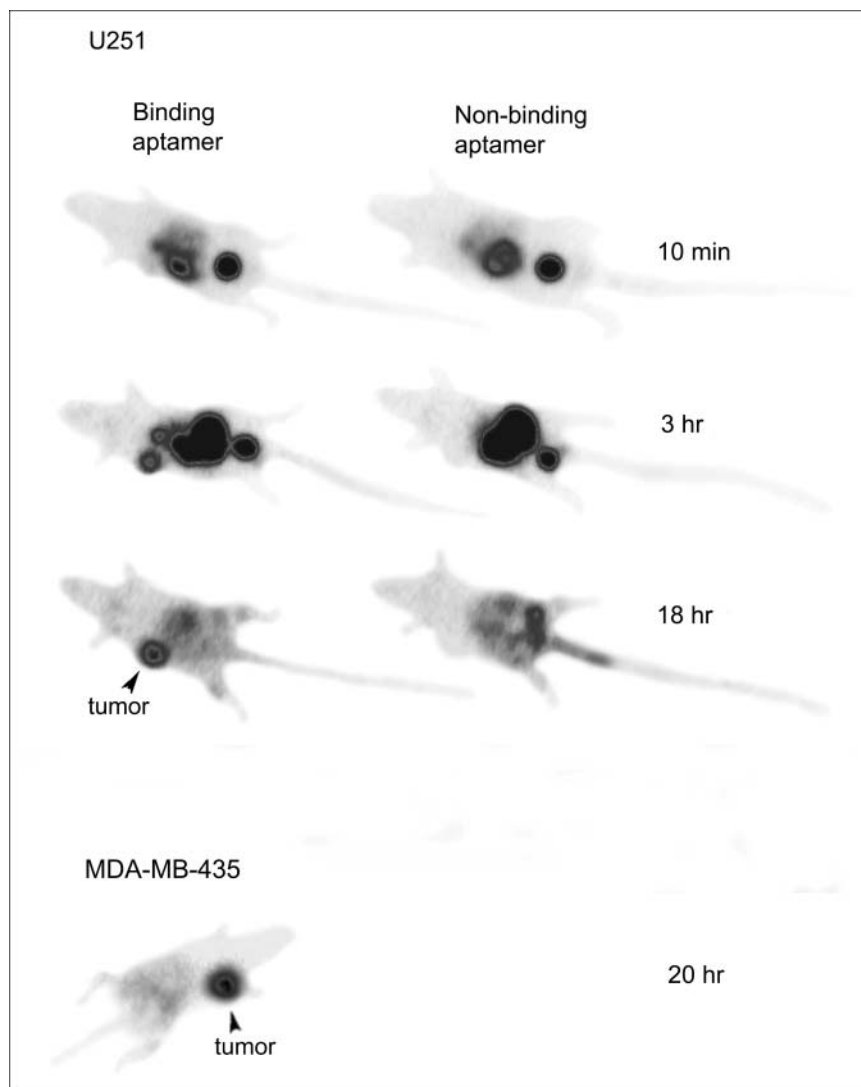


FIGURE 6. Aptamer-based γ -camera images of tumors. With binding aptamer but not with control aptamer, U251 glioblastoma tumor is faintly visible at 10 min, prominent at 3 h, and the brightest structure at 18 h. Structures prominent at 10 min include bladder and visceral mass. Large intestine, bladder, and tumor are seen at 3 h. Also tested was MDA-MB-435 breast tumor implanted into mammary fat pad of female nude mice and allowed to grow to 400 mg. TTA1 was labeled with ^{99m}Tc , injected intravenously at 3.25 mg/kg, and imaged at 20 h.

clearance patterns, indicating that aptamer properties can be tailored to address different needs. Chemical synthesis enables facile, site-specific conjugation to a variety of inert and bioactive molecules, smoothing transitions between

discovery, research, and clinical applications. Given the variety of human pathologic states that express high levels of tenascin-C, the properties of aptamer TTA1 are a topic of ongoing interest.

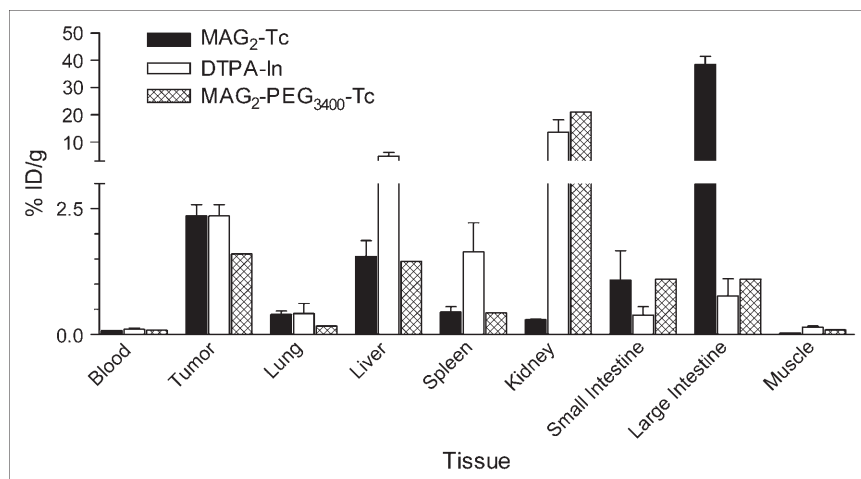


FIGURE 7. Bar graph showing effect of radiometal chelator on biodistribution. Data are mean \pm SE ($n = 3$), except for MAG₂-PEG_{3,400} ($n = 2$). Lg. = large; Sm. = small.

ACKNOWLEDGMENTS

We thank Liz Chlipala and Alison Bendele of BolderPath (now at Premier Histology and BolderBioPath, respectively) for assistance with tissue sections and fluorescence microscopy. Dave Schneider, Jeff Walenta, and Philippe Bridonneau performed oligonucleotide synthesis and purification, and Blake Tomkinson, Jeremy LeRay, Eric Brown, and David Emerson provided cell culture expertise and mouse tumor xenografts. Prof. Luciano Zardi (Istituto Nazionale per la Ricerca sul Cancro, Genoa, Italy) and Prof. Harold Erickson (Duke University, Durham, NC) generously provided antitenascin antibodies. We thank colleagues at Schering AG (Berlin), including Dietmar Berndorff, Ludger Dinkelborg, and Prof. Ullrich Speck, for many helpful discussions, and Drew Smith and Mathias Friebe for helpful comments on the manuscript.

REFERENCES

- Wu AM, Chen W, Raubitschek A, et al. Tumor localization of anti-CEA single-chain Fvs: improved targeting by non-covalent dimers. *Immunotechnology*. 1996;2:21–36.
- Adams GP, Schier R, McCall AM, et al. Prolonged in vivo tumour retention of a human diabody targeting the extracellular domain of human her2/neu. *Br J Cancer*. 1998;77:1405–1412.
- Lister-James J, Moyer BR, Dean T. Small peptides radiolabeled with ^{99m}Tc. *Q J Nucl Med*. 1996;40:221–233.
- Boerman OC, Kranenborg MH, Oosterwijk E, et al. Pretargeting of renal cell carcinoma: improved tumor targeting with a bivalent chelate. *Cancer Res*. 1999;59:4400–4405.
- Paganelli G, Grana C, Chinol M, et al. Antibody-guided three-step therapy for high grade glioma with yttrium-90 biotin. *Eur J Nucl Med*. 1999;26:348–357.
- Gold L, Polisky B, Uhlenbeck O, Yarus M. Diversity of oligonucleotide functions. *Annu Rev Biochem*. 1995;64:763–797.
- Famulok M, Mayer G. Aptamers as tools in molecular biology and immunology. *Curr Top Microbiol Immunol*. 1999;243:123–136.
- Watson SR, Chang YF, O'Connell D, Weigand L, Ringquist S, Parma DH. Anti-L-selectin aptamers: binding characteristics, pharmacokinetic parameters, and activity against an intravascular target in vivo. *Antisense Nucleic Acid Drug Dev*. 2000;10:63–75.
- Ruckman J, Green LS, Beeson J, et al. 2'-fluoropyrimidine RNA-based aptamers to the 165-amino acid form of vascular endothelial growth factor (VEGF165): inhibition of receptor binding and VEGF-induced vascular permeability through interactions requiring the exon 7-encoded domain. *J Biol Chem*. 1998;273:20556–20567.
- Eyeteck Study Group. Anti-vascular endothelial growth factor therapy for subfoveal choroidal neovascularization secondary to age-related macular degeneration: phase II study results. *Ophthalmology*. 2003;110:979–986.
- Guhlke S, Famulok M, Biersack HJ. Aptamers: a novel class of radiopharmaceutical with diagnostic and therapeutic potential. *Eur J Nucl Med Mol Imaging*. 2003;30:1441–1443.
- Hicke BJ, Stephens AW. Escort aptamers: a delivery service for diagnosis and therapy. *J Clin Invest*. 2000;106:923–928.
- Cerchia L, Hamm J, Libri D, Tavitian B, de Franciscis V. Nucleic acid aptamers in cancer medicine. *FEBS Lett*. 2002;528:12–16.
- Charlton J, Sennello J, Smith D. In vivo imaging of inflammation using an aptamer inhibitor of human neutrophil elastase. *Chem Biol*. 1997;4:809–816.
- Zhang YM, Liu N, Zhu ZH, Ruszkowski M, Hnatowich DJ. Influence of different chelators (HYNIC, MAG₃ and DTPA) on tumor cell accumulation and mouse biodistribution of technetium-99m labeled antisense DNA. *Eur J Nucl Med*. 2000;27:1700–1707.
- Tavitian B, Terrazzino S, Kuhnast B, et al. In vivo imaging of oligonucleotides with positron emission tomography. *Nat Med*. 1998;4:467–471.
- Hicke BJ, Marion C, Chang YF, et al. Tenascin-c aptamers are generated using tumor cells and purified protein. *J Biol Chem*. 2001;276:48644–48654.
- Zagzag D, Friedlander DR, Miller DC, et al. Tenascin expression in astrocytomas correlates with angiogenesis. *Cancer Res*. 1995;55:907–914.
- Erickson HP, Bourdon MA. Tenascin: an extracellular matrix protein prominent in specialized embryonic tissues and tumors. *Annu Rev Cell Biol*. 1989;5:71–92.
- Koukoulis GK, Gould VE, Bhattacharyya A, Gould JE, Howedy AA, Virtanen I. Tenascin in normal, reactive, hyperplastic, and neoplastic tissues: biologic and pathologic implications. *Hum Pathol*. 1991;22:636–643.
- Mackie EJ, Halfter W, Liverani D. Induction of tenascin in healing wounds. *J Cell Biol*. 1988;107:2757–2767.
- Wallner K, Li C, Shah PK, et al. Tenascin-c is expressed in macrophage-rich human coronary atherosclerotic plaque. *Circulation*. 1999;99:1284–1289.
- Lightner VA, Slemp CA, Erickson HP. Localization and quantitation of hexabrachion (tenascin) in skin, embryonic brain, tumors, and plasma. *Ann N Y Acad Sci*. 1990;580:260–275.
- Lastoria S, Castelli L, Vergara E, et al. Human gliomas radioimmunoimaging with ¹³¹I BC-2 murine IgG: preliminary report. *J Nucl Med Allied Sci*. 1990;34:173–176.
- Paganelli G, Magnani P, Zito F, et al. Pre-targeted immunodetection in glioma patients: tumour localization and single-photon emission tomography imaging of [^{99m}Tc]PNAO-biotin. *Eur J Nucl Med*. 1994;21:314–321.
- Daniels DA, Chen H, Hicke BJ, Swiderik KM, Gold L. A tenascin-c aptamer identified by tumor cell SELEX: systematic evolution of ligands by exponential enrichment. *Proc Natl Acad Sci U S A*. 2003;100:15416–15421.
- Green LS, Jellinek D, Bell C, et al. Nuclease-resistant nucleic acid ligands to vascular permeability factor/vascular endothelial growth factor. *Chem Biol*. 1995;2:683–695.
- Hilger CS, Willis MC, Wolters M, Pieken WA. Tc-99m-labeling of modified RNA. *Nucleosides Nucleotides*. 1999;18:1479–1481.
- Bridonneau P, Bunch S, Tengler R, et al. Purification of a highly modified RNA-aptamer: effect of complete denaturation during chromatography on product recovery and specific activity. *J Chromatogr B Biomed Sci Appl*. 1999;726:237–247.
- Dewanjee MK, Ghafouripour AK, Kapadvanjwala M, et al. Noninvasive imaging of c-myc oncogene messenger RNA with indium-111-antisense probes in a mammary tumor-bearing mouse model. *J Nucl Med*. 1994;35:1054–1063.
- Balza E, Siri A, Ponassi M, et al. Production and characterization of monoclonal antibodies specific for different epitopes of human tenascin. *FEBS Lett*. 1993;332:39–43.
- Fujimori K, Covell DG, Fletcher JE, Weinstein JN. Modeling analysis of the global and microscopic distribution of immunoglobulin G, F(ab')₂, and Fab in tumors. *Cancer Res*. 1989;49:5656–5663.
- Juweid M, Neumann R, Paik C, et al. Micropharmacology of monoclonal antibodies in solid tumors: direct experimental evidence for a binding site barrier. *Cancer Res*. 1992;52:5144–5153.
- Hassfjell S, Brechbiel MW. The development of the alpha-particle emitting radionuclides ²¹²Pb and ²¹³Pb, and their decay chain related radionuclides, for therapeutic applications. *Chem Rev*. 2001;101:2019–2036.
- Tarli L, Balza E, Viti F, et al. A high-affinity human antibody that targets tumoral blood vessels. *Blood*. 1999;94:192–198.
- Borsi L, Carnemolla B, Nicolo G, Spina B, Tanara G, Zardi L. Expression of different tenascin isoforms in normal, hyperplastic and neoplastic human breast tissues. *Int J Cancer*. 1992;52:688–692.
- Healy JM, Lewis SD, Kurz M, et al. Pharmacokinetics and biodistribution of novel aptamer compositions. *Pharm Res*. 2004;21:2234–2246.
- Tsai SW, Li L, Williams LE, Anderson AL, Raubitschek AA, Shively JE. Metabolism and renal clearance of ¹¹¹In-labeled DOTA-conjugated antibody fragments. *Bioconjug Chem*. 2001;12:264–270.
- Rogers BE, Franano FN, Duncan JR, et al. Identification of metabolites of ¹¹¹In-diethylenetriaminepentaacetic acid-monoclonal antibodies and antibody fragments in vivo. *Cancer Res*. 1995;55:5714s–5720s.
- Arano Y. Strategies to reduce renal radioactivity levels of antibody fragments. *Q J Nucl Med*. 1998;42:262–270.



The Journal of
NUCLEAR MEDICINE

Tumor Targeting by an Aptamer

Brian J. Hicke, Andrew W. Stephens, Ty Gould, Ying-Fon Chang, Cynthia K. Lynott, James Heil, Sandra Borkowski, Christoph-Stephan Hilger, Gary Cook, Stephen Warren and Paul G. Schmidt

J Nucl Med. 2006;47:668-678.

This article and updated information are available at:
<http://jnm.snmjournals.org/content/47/4/668>

Information about reproducing figures, tables, or other portions of this article can be found online at:
<http://jnm.snmjournals.org/site/misc/permission.xhtml>

Information about subscriptions to JNM can be found at:
<http://jnm.snmjournals.org/site/subscriptions/online.xhtml>

The Journal of Nuclear Medicine is published monthly.
SNMMI | Society of Nuclear Medicine and Molecular Imaging
1850 Samuel Morse Drive, Reston, VA 20190.
(Print ISSN: 0161-5505, Online ISSN: 2159-662X)

© Copyright 2006 SNMMI; all rights reserved.